Available online at www.sciencedirect.com
ScienceDirect
Trans. Nonferrous Met. Soc. China 32(2022) 3744−3752
Transactions of Nonferrous Metals Society of China
www.tnmsc.cn

Galvanic effect of magnetite on electrochemical oxidation of arsenopyrite in acidic culture medium

Sha DENG[1], Guo-hua GU[2], Tao LONG[1], Wei XIAO[1], Wei YANG[1]

1. School of Resources Engineering, Xi'an University of Architecture and Technology, Xi'an 710055, China;
2. School of Minerals Processing and Bioengineering, Central South University, Changsha 410083, China

Received 22 August 2021; accepted 30 December 2021

Abstract: The galvanic interaction of arsenopyrite−magnetite in acidic culture medium was investigated by electrochemical measurements, X-ray photoelectron spectroscopy characterization and leaching experiments. The results indicated that the rest potential of magnetite was 321 mV, which was more anodic than 223 mV of arsenopyrite, and the galvanic current was 7.40 μA, verifying the existence of the galvanic interaction between arsenopyrite and magnetite. The galvanic potential and polarization curves suggested that the redox behaviors of arsenopyrite dominated the overall galvanic interaction. The galvanic interaction enhanced the electrochemical dissolution of arsenopyrite with the generation of more oxidation products (S^0, SO_3^{2-}, SO_4^{2-} and AsO_3^{3-}) on arsenopyrite and an increase in the chemical reactivity of the surface. Leaching experiments of 6 days showed that the presence of magnetite improved the arsenic release from arsenopyrite by 30 mg/L, and further confirmed the enhanced oxidation of arsenopyrite when coupled with magnetite.

Key words: arsenopyrite; magnetite; galvanic interaction; electrochemistry; surface properties; leaching

1 Introduction

The development of the social economy contributes to the continuously decreasing reserves of easy-leaching gold ores, and the refractory ones have become the most critical gold resources in the world [1,2]. Gold particles are often "invisible" and trapped in arsenopyrite and pyrite [3]. Biological oxidation is considered as an effective and efficient pretreatment method to render the contained gold released [4−6]. However, sometimes the gold recovery could not be ensured because of the low dissolution of arsenopyrite. One of the most important factors associated with the low dissolution of arsenopyrite might be the toxicity of As(III) and As(V) to the microorganisms, since the formation of As(III) and As(V) is inevitable during the leaching of arsenopyrite. Another factor is the passivation product covering on the mineral surface, which hinders the further dissolution of arsenopyrite. Elemental sulfur, jarosite, and scorodite have been reported as components of the passivation layers accumulated on the arsenopyrite surface [7,8].

A lot of researches have been carried out on developing methods to promote arsenopyrite leaching, involving using thermophilic microorganisms or mixed strains [9−11], adding ferric ions or cupric ions [12−14], designing new bioreactors to maintain the high bioactivity of microorganisms at high pulp densities [15], and adding another noble mineral to form a galvanic cell [16−18].

One of the most studied galvanic interactions with arsenopyrite is the pyrite−arsenopyrite interaction. In nature, usually pyrite has a close inter-growth with arsenopyrite in refractory gold

Corresponding author: Wei YANG, Tel: +86-15009267016, E-mail: yangweixauat@126.com
DOI: 10.1016/S1003-6326(22)66054-0

ores. TAXIARCHOU et al [19] observed that arsenopyrite was oxidized at 480−550 mV, and pyrite was oxidized at more anodic potentials where the oxidation of arsenopyrite had almost ceased. KOMNITSAS et al [20] concluded that arsenopyrite was oxidized more preferentially as compared with pyrite. URBANO et al [21] found that the electrochemical reactivity of pyrite contained in arsenopyrite was delayed in 0.1 mol/L $NaNO_3$ electrolyte (pH=6.5). DOS SANTOS et al [22] reported that pyrite contributed more to the valence band of the pyrite−arsenopyrite solid/solid interface, whereas arsenopyrite contributed more to the conduction band. That shifted the valence state positively and reduced the band gap, and thus facilitated the interfacial electron transfer. XU et al [23] proposed that the corrosion behavior of the galvanic pair agreed with that of arsenopyrite. Additionally, the galvanic interaction increased the anodic and cathodic current densities and decreased the electron transfer resistance, contributing to the accelerated corrosion of arsenopyrite. In our previous studies [17,24], it is found that apart from the galvanic interaction, the low crystallinity of the product layers generated on the surface of arsenopyrite in the presence of pyrite is also the reason for the promoted leaching of arsenopyrite.

Magnetite follows an inverse spinel structure with the chemical formula of $B(AB)O_4$ where ferrous ions occupy half of the octahedral lattice sites, and ferric ions occupy the other half of the octahedral lattice sites and all the tetrahedral lattice sites. Electrons coordinated with these iron species are thermally delocalized and can migrate rapidly within the magnetite lattice, and hence magnetite exhibits excellent electrical conductivity [25]. Therefore, a galvanic cell can be formed when it contacts with sulfide minerals with semiconductive properties. The galvanic interaction between magnetite and chalcopyrite has been confirmed in a previous study [26]. Since it can be recycled for the stable structure and strong magnetism, magnetite would be an ideal cathode material which can be used to galvanically enhance arsenopyrite leaching.

However, at present, few efforts have been made to investigate the galvanic effect of magnetite on the oxidation of arsenopyrite. In this study, the galvanic interaction between arsenopyrite and magnetite was systematically studied in acidic culture medium by some alternative electrochemical techniques, X-ray photoelectron spectroscopy (XPS) and leaching experiments. The objective is to confirm the galvanic interaction between arsenopyrite and pyrite, and then to provide an innovative approach for efficient pretreatment of refractory gold ores.

2 Experimental

2.1 Minerals

The arsenopyrite samples were obtained from Inner Mongolia, China. The samples were prepared by crushing, hand-sorting to remove the gangue minerals, grinding and dry-sieving to 0.037−0.074 mm. The magnetite samples were obtained from Changsha Research Institute of Mining and Metallurgy (China), with the particle diameter smaller than 0.037 mm. The XRD patterns of arsenopyrite and magnetite samples are shown in Fig. 1. Quantitative XRD analysis indicated that the purities of both samples were higher than 95%.

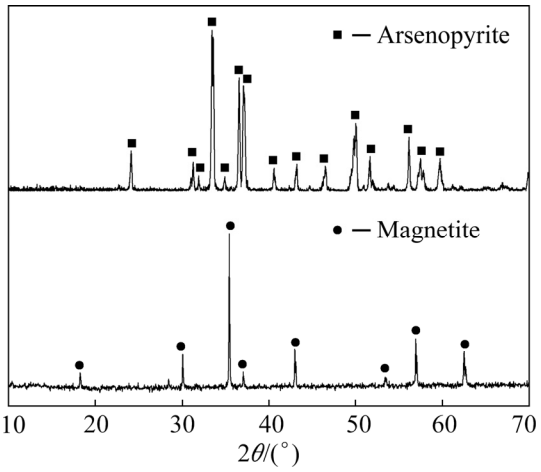

Fig. 1 XRD patterns of arsenopyrite and magnetite samples

2.2 Electrochemical experiments

2.2.1 Working electrodes preparation

The working electrode used in this work was a carbon-paste electrode bound with paraffin wax. 2.1 g of mineral samples and 0.6 g of graphite were mixed with 0.3 g of paraffin wax which was melted in a 50 mL beaker by an alcohol burner. The paste was then compacted in a cylindrical chrome steel mold with a diameter of 15 mm under a pressure of 35 MPa for 10 min. The compressed cylinder was sealed in a PTFE sample holder, with an area of 1 cm^2 exposed to the electrolyte. Before each test,

the working electrode was sequentially abraded with 600#, 1000# and 1500# silicon carbide paper, and rinsed with distilled water and ethyl alcohol several times, in order to create a fresh working surface.

2.2.2 Electrochemical measurements

All the electrochemical experiments were carried out on the Zahner Zennium E potentiostat (Germany) equipped with a computer. The electrochemical cell was a glass reactor with an effective volume of 200 mL. A conventional three-electrode electrochemical system was applied in this research. A saturated $Hg/HgCl_2$ electrode (SCE) was used as the reference electrode (241.5 mV vs SHE, 25 °C). The auxiliary electrode was a graphite electrode. The iron-free 9K medium at pH=2 was used as the electrolyte solution. All the chemical reagents used in this study were of analytical grade.

The rest potentials (open circuit potential, OCP) of arsenopyrite and magnetite were measured with the freshly prepared working electrodes in open circuit mode for 30 min. The galvanic potential between arsenopyrite and magnetite was measured by short-circuiting both working electrodes by an electric wire and recording the potential in the same way as the rest potential measurement. The galvanic current measurement was performed in a two-electrode electrochemical cell where arsenopyrite was connected to the working electrode clip, whereas magnetite was connected to the auxiliary/reference electrode clip, as shown in Fig. 2. The potential between them was set to be 0 V, and in this manner, the potentiostat could be regarded as a zero-resistance ammeter (ZRA).

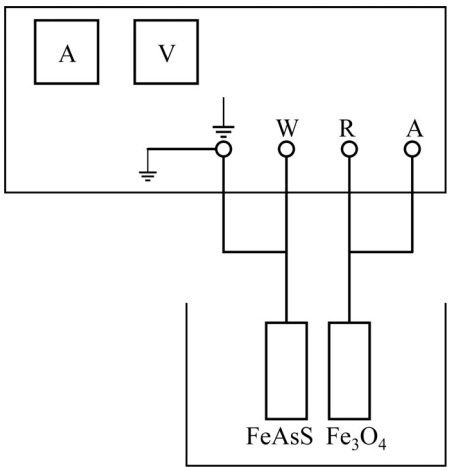

Fig. 2 Schematic set-up for measuring galvanic current

Tafel polarization curves were measured in the potential range of OCP ± 250 mV with a sweep rate of 1 mV/s. Tafel slopes (anodic and cathodic), corrosion current density and polarization resistance were calculated by the Zahner Analysis software in the potential range of 50−100 mV away from the corrosion potential. The cyclic voltammetry measurements were performed from OCP to −600 mV (negative-going potential scan), then reversed to 600 mV (positive-going potential scan) and back to OCP with a scan rate of 20 mV/s. All the potentials reported in this work were with respect to SCE, and all the measurements were conducted in the stationary state without removing oxygen and in triplicate.

2.3 X-ray photoelectron spectroscopy

XPS was used to identify the surface species of arsenopyrite electrodes after self-corrosion and galvanic corrosion with magnetite for 24 h. The reason for corrosion of 24 h not 2 h was to amplify the difference of surface properties of arsenopyrite after self-corrosion and galvanic corrosion. The XPS spectra of the arsenopyrite surfaces were collected using a PHI5000 VersaprobeIII X-ray photoelectron spectrometer (ULVAC−PHI) with mono Al K_α X-rays (1486.6 eV) at 15 kV and 4.5 mA, and was processed with Multipak 9.6. All the spectra were fitted and calculated after aligning C 1s peak to 284.8 eV.

2.4 Leaching experiments

Leaching experiments were performed in 250 mL flasks with 150 mL iron-free 9K medium whose composition was 3 g/L $(NH_4)_2SO_4$, 0.5 g/L K_2HPO_4, 0.5 g/L $MgSO_4·7H_2O$, 0.01 g/L $Ca(NO_3)_2$ and 0.1g/L KCl. The initial pH was adjusted to 2.0 with 20% sulfuric acid. 1.5 g of arsenopyrite or 1.5 g of arsenopyrite and 0.5 g of magnetite were added to each flask. The rotating speed and temperature of the incubator were set to be 165 r/min and 35 °C, respectively. Each experiment was conducted in duplicate. 1 mL of leaching solution was sampled every day to analyze the total arsenic concentration. The sampling loss was compensated with 1 mL of the iron-free medium. Evaporation loss was supplemented with distilled water at pH=2.0. The total arsenic concentration was determined by an atomic fluorescence spectrometer.

3 Results and discussion

3.1 Galvanic potential and current of arsenopyrite−magnetite couple

Figure 3 shows the rest potentials of arsenopyrite and magnetite electrodes in iron-free 9K medium (pH=2) during the immersion time of 30 min. Variations of the rest potentials resulted from the rearrangement of electric charges in the double-layer capacitance formed at the electrode/electrolyte interface and chemical reactions at the interface. The stable rest potentials of arsenopyrite and magnetite were 223 and 321 mV, respectively, with a difference of 98 mV. This suggests that arsenopyrite is more reactive than magnetite in sulfuric acid, and therefore they can form a galvanic cell in which arsenopyrite with lower rest potential acts as the anode and magnetite with higher rest potential as the cathode. The galvanic potential between arsenopyrite and magnetite was stabilized at 230 mV, which sat between the rest potentials of arsenopyrite and magnetite. Since the galvanic potential represents the new equilibrium point of the arsenopyrite−magnetite couple and the galvanic potential is more positive than the rest potential of arsenopyrite, the galvanic interaction can result in the anodic polarization of the arsenopyrite electrode, contributing to the accelerated oxidation of arsenopyrite. Additionally, the galvanic potential was only 7 mV larger than the rest potential of arsenopyrite. This means that the redox behaviors of arsenopyrite play a dominant role in the galvanic interaction between arsenopyrite and magnetite.

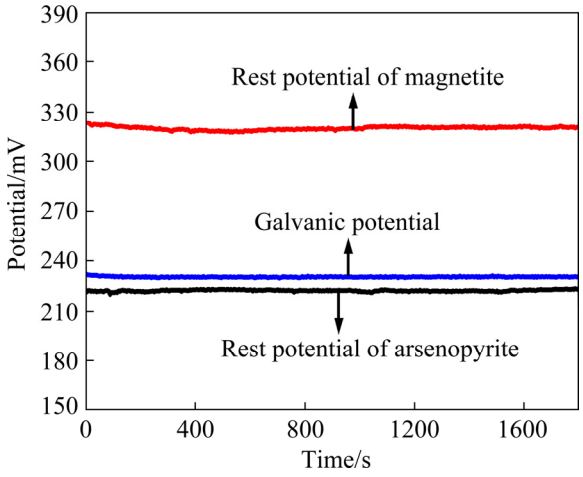

Fig. 3 Rest potentials of arsenopyrite and magnetite and galvanic potential of arsenopyrite−magnetite couple

Figure 4 shows the galvanic current of the arsenopyrite−magnetite couple and the self-corrosion current of arsenopyrite. The galvanic current had a rapid drop in the initial stage due to the transient charge of the double-layer electrical capacitance [27], and then reached a plateau that was the desired galvanic current. The galvanic current in the medium was 7.40 μA, demonstrating that the arsenopyrite electrode was the anodic component of the galvanic couple. The self-corrosion current of arsenopyrite was approximately zero, which was lower than the galvanic current, confirming that the oxidation of arsenopyrite can be enhanced when galvanically coupled with magnetite.

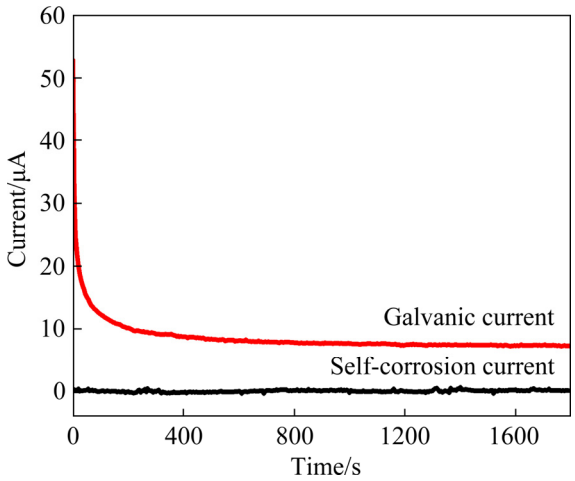

Fig. 4 Galvanic current for arsenopyrite−magnetite couple

3.2 Tafel polarization plots

Apart from corrosion potential (φ_{corr}), Tafel polarization curves can provide a lot of useful kinetics information, such as corrosion current density (J_{corr}), Tafel slopes and polarization resistance (R_p). Figure 5 presents the Tafel polarization curves of arsenopyrite, magnetite and arsenopyrite−magnetite galvanic couple in the iron-free 9K medium. The φ_{corr} of magnetite was 221 mV, which was higher than 161 mV of arsenopyrite. The φ_{corr} of the galvanic couple was 173 mV, which sat between the φ_{corr} values of arsenopyrite and magnetite. These observations were consistent with the rest potential results. The cathodic curves for arsenopyrite and arsenopyrite−magnetite couple showed a similar reduction behavior, but the cathodic current density for the couple was much larger than that for arsenopyrite.

Due to the linear relationship between the reaction rate and the current density, it is apparent that the galvanic coupling with magnetite promoted the cathodic reduction of arsenopyrite. By contrast, the anodic curve of the galvanic couple overlapped with that of arsenopyrite, implying that the anodic oxidation of arsenopyrite dominated the galvanic interaction.

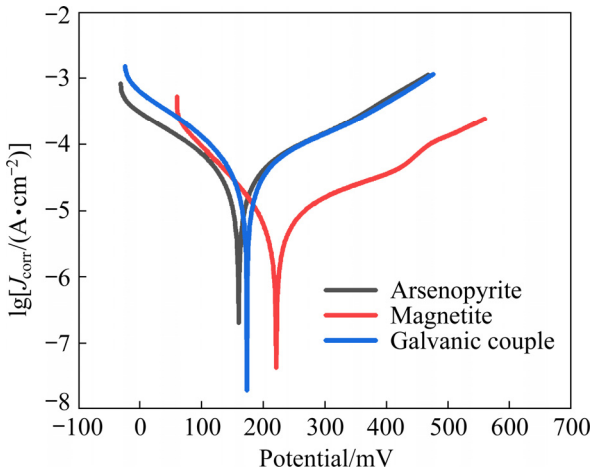

Fig. 5 Tafel polarization curves of arsenopyrite, magnetite and arsenopyrite−magnetite galvanic couple

As listed in Table 1, the J_{corr} of the arsenopyrite electrode (32.32 μA/cm^2) was remarkably larger than that of magnetite (5.80 μA/cm^2), confirming that magnetite was much more inert than arsenopyrite. As for the arsenopyrite−magnetite couple, a higher J_{corr} of 43.23 μA/cm^2 was obtained, as compared with 32.32 μA/cm^2 of arsenopyrite, suggesting that the galvanic interaction with magnetite would contribute to the improved dissolution of arsenopyrite, which was also confirmed by the polarization resistances (R_p). Combining with the shape of the polarization curves, the galvanically promoted dissolution of arsenopyrite was mainly associated with the enhanced cathodic reduction in the presence of magnetite.

3.3 Cyclic voltammograms

In order to further illustrate the influence of the galvanic interaction with magnetite on the surface properties of arsenopyrite, the cyclic voltammograms of arsenopyrite were measured after self-corrosion and galvanic corrosion for 2 h, and the results are shown in Fig. 6. The cyclic voltammogram scans started negatively from OCP to −600 mV, then reversed to 600 mV, and finally back to OCP.

The detailed oxidation and reduction process of arsenopyrite has been discussed in our previous study [28]. The broad cathodic Peak C between 0 and −200 mV was associated with the reduction of elemental sulfur, accompanied with the formation of H_2S (Eq. (4)). It is noted that the cathodic current density of Peak C after galvanic corrosion with magnetite was a little larger as compared with that after self-corrosion, suggesting that the galvanic interaction with magnetite contributed to the generation of more elemental sulfur on the arsenopyrite surface. The anodic oxidation Peak A corresponded to the oxidation of arsenopyrite, as described in Eqs. (1)−(3). It is notable that the anodic current density after galvanic coupling was much higher as compared with that after self-oxidation. This means the presence of magnetite increased the chemical reactivity of the arsenopyrite surface, which might be related to the more oxidation products (S^0 and AsO_3^{3-}) formed on the arsenopyrite surface. The cathodic Peak B was related to the reduction of Fe^{3+} to Fe^{2+}.

$$FeAsS + 3H_2O \rightarrow Fe^{2+} + AsO_3^{3-} + S^0 + 6H^+ + 5e \quad (1)$$

$$Fe^{2+} \rightarrow Fe^{3+} + e \quad (2)$$

$$S^0 + 4H_2O \rightarrow 8H^+ + SO_4^{2-} + 6e \quad (3)$$

$$S^0 + 2H^+ + 2e \rightarrow H_2S \quad (4)$$

To sum up, differences of cyclic voltammograms between arsenopyrite after self-corrosion and galvanic interaction with magnetite are in good

Table 1 Electrochemical kinetics parameters calculated from polarization curves

Electrode	φ_{corr}/mV	J_{corr}/(μA·cm^{-2})	b_a/(mV·decade^{-1})	b_c/(mV·decade^{-1})	R_p/kΩ
Arsenopyrite	161	32.32	202	161	1.20
Magnetite	221	5.80	180	97.3	4.73
Galvanic couple	173	43.23	242	146	0.91

b_a and b_c are the anodic and cathodic Tafel slopes in the Butler−Volmer equation, $J = J_{corr}[\exp(2.3\eta/b_a) - \exp(-2.3\eta/b_c)]$, and η is the over potential; R_p refers to the linear polarization resistance for corrosion, $R_p = b_a b_c/[2.3(b_a + b_c)J_{corr}]$.

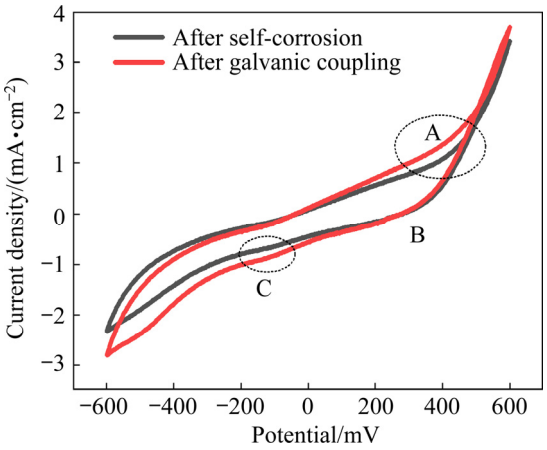

Fig. 6 Cyclic voltammograms of arsenopyrite after self-oxidation and galvanic coupling with magnetite for 2 h

accordance with the galvanic current and polarization curves results. This confirms that the galvanic effect between arsenopyrite and magnetite can alter the arsenopyrite surface with the generation of more oxidation products and an increase in the chemical reactivity of the arsenopyrite surface.

3.4 XPS characterization

Figure 7 displays the S 2p and As 3d XPS spectra of arsenopyrite with and without galvanic coupling with magnetite. The contents of each surface species calculated from the spectra are listed in Table 2. Due to the high intensity of C 1s and the thickness of the arsenopyrite electrode, the Fe 2p spectra did not show any signals of energy peaks, and therefore the Fe 2p spectra are not presented in this study.

The S 2p spectra of arsenopyrite were fitted with 5 doublet peaks. Because of the high similarity between the binding energy peaks of $(AsS)^{2-}$ and S_2^{2-} [29], the peaks of $(AsS)^{2-}$ represent the sum of $(AsS)^{2-}$ and S_2^{2-} in this study. According to the binding energies of each sulfur species reported in previous studies [29,30], the peaks around 161.25 eV are representative of S^{2-}, and the peaks around 162.7 eV refer to $(AsS)^{2-}$. The energy regions around 163.7 eV represent S_n^{2-}/S^0. The higher regions around 165.8 and 168.3 eV correspond to S from SO_3^{2-} and SO_4^{2-}, respectively. As for the arsenopyrite surface after self-oxidation, the $(AsS)^{2-}$ and S_n^{2-}/S^0 were the major chemical states of sulfur, which accounted for 30.25% and 32.88%, respectively, and the sum of the contents of SO_3^{2-} and SO_4^{2-} was 25.36%. After galvanic coupling with magnetite, the content of $(AsS)^{2-}$ decreased to 19.81%, and SO_3^{2-} and SO_4^{2-} increased to a proportion of 34.55% in total. This indicates that the galvanic interaction with magnetite enhanced the oxidation of arsenopyrite and resulted in the generation of more oxidation products on the surface of arsenopyrite. It is noticeable that the content of S_n^{2-}/S^0 after galvanic coupling (32.45%) had no obvious difference from that after self-

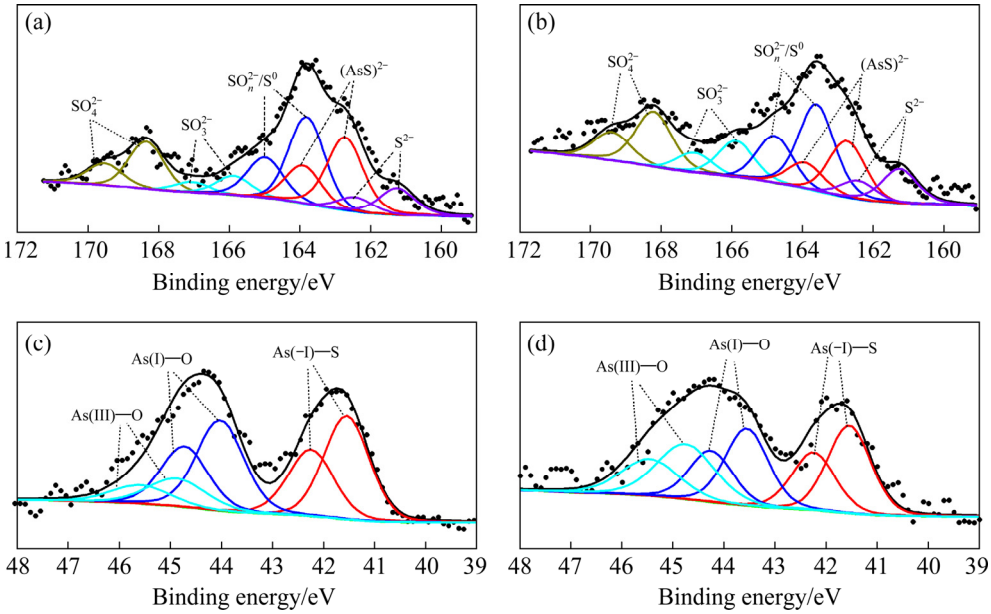

Fig. 7 XPS spectra of arsenopyrite after self-corrosion (a, c) and galvanic corrosion (b, d) for 24 h: (a, b) S 2p; (c, d) As 3d

Table 2 Contents of each chemical state of sulfur and arsenic on arsenopyrite surfaces after self-corrosion and galvanic coupling with magnetite for 24 h

Species		Arsenopyrite after self-corrosion		Arsenopyrite after galvanic coupling	
		Binding energy/eV	Content/%	Binding energy/eV	Content/%
S 2p	S^{2-}	161.25	11.51	161.25	13.19
	$(AsS)^{2-}$	162.72	30.25	162.74	19.81
	S_n^{2-}/S^0	163.81	32.88	163.61	32.45
	SO_3^{2-}	165.87	7.71	165.88	13.41
	SO_4^{2-}	168.35	17.65	168.21	21.14
As 3d	As(−I)—S	41.55	43.38	41.55	36.28
	As(I)—O	44.03	41.03	43.56	32.41
	As(III)—O	44.88	15.59	44.75	31.30

oxidation (32.88%). This contradicts with cyclic voltammograms in which more elemental sulfur was detected after coupling with magnetite. This might be attributed to that some of elemental sulfur was oxidized to SO_3^{2-} and SO_4^{2-} after a longer time (24 h) of oxidation, confirmed by the larger proportion of SO_3^{2-} and SO_4^{2-} on arsenopyrite.

Three doublet peaks were used to fit the As 3d spectra. The energy peaks around 41.55 eV are representative of As(−I)—S from the bulk arsenopyrite [29,30]. The higher regions around 43.8 and 44.8 eV are interpreted as As(I)—O and As(III)—O, respectively. The content of As(−I)—S on arsenopyrite after galvanic coupling was 36.28%, which was lower than that after self-oxidation (43.38%). In addition, 31.30% of arsenic on arsenopyrite after galvanic interaction was in the form of As(III)—O, but the proportion of As(III)—O after self-oxidation was only 15.59%. These observations further prove that the presence of magnetite contributed to the promoted oxidation of arsenopyrite with additional AsO_3^{3-} species accumulated on the surface of arsenopyrite.

3.5 Leaching results

To further confirm the promoted dissolution of arsenopyrite in the presence of magnetite, leaching experiments of arsenopyrite with/without magnetite were conducted in the iron-free 9K medium of pH 2, and the total arsenic concentrations in the solution during the leaching of 5 days are shown in Fig. 8(a). It is notable that after leaching for 5 days, about 240 mg/L arsenic was extracted for pure arsenopyrite, but in the presence of magnetite, nearly 270 mg/L of arsenic concentration was obtained, verifying that the presence of magnetite accelerated the dissolution of arsenopyrite. The oxidation of arsenopyrite in the acidic culture medium is a very slow chemical reaction, and the generation of ferric ions is very difficult. Therefore, the addition of magnetite did not exert any effect on the redox potential during arsenopyrite leaching, as shown in Fig. 8(b).

It is evident that the difference imposed by the galvanic coupling with magnetite was not

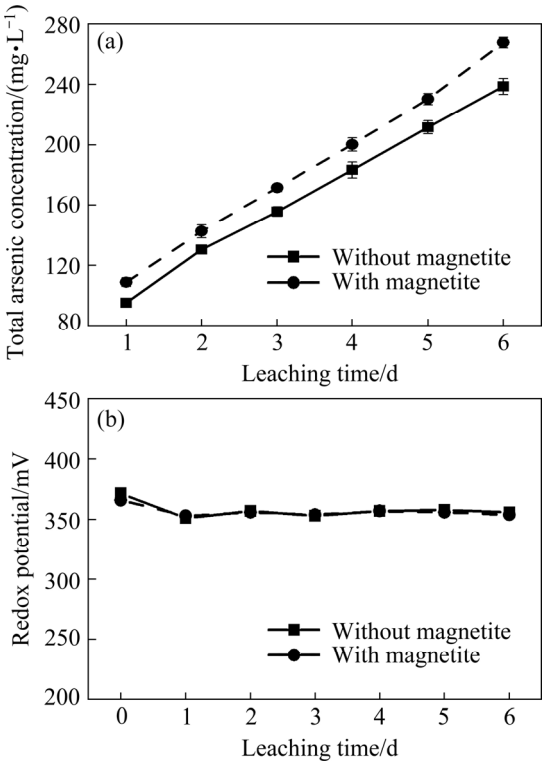

Fig. 8 Influence of magnetite on total arsenic concentration (a) and redox potential (b) during arsenopyrite leaching in acidic culture medium (pH=2)

significant. This might be attributed to the mild feature of the culture medium or the improper mass ratio of arsenopyrite to magnetite. Therefore, the galvanic interaction between arsenopyrite and magnetite in the presence of ferric ions or iron-oxidizing/sulfur-oxidizing microorganisms will be further studied. Additionally, it is essential to investigate the influence of the mass ratio of magnetite to arsenopyrite on the leaching behaviors of arsenopyrite.

4 Conclusions

(1) The galvanic pair of arsenopyrite−magnetite in acidic culture medium (iron-free 9K medium of pH 2) was identified. Arsenopyrite with lower rest potential acts as the anode, and magnetite with higher rest potential acts as the cathode. The galvanic potential was higher than the rest potential of arsenopyrite, and thus the galvanic coupling with magnetite resulted in the anodic polarization of arsenopyrite, facilitating the dissolution of arsenopyrite.

(2) Compared with arsenopyrite after self-oxidation, more oxidation products (S^0, SO_3^{2-}, SO_4^{2-} and AsO_3^{3-}) were detected on the surface of arsenopyrite after galvanic coupling with magnetite, as cyclic voltammograms and XPS characterizations revealed. Cyclic voltammograms also proved that the galvanic interaction with magnetite increased the chemical reactivity of the arsenopyrite surface.

(3) Leaching experiments further confirmed the promoted oxidation of arsenopyrite when coupled with magnetite. This study would provide an innovative approach for the efficient leaching of arsenopyrite and other refractory sulfide minerals.

Acknowledgments

The authors are grateful for the financial supports from the Natural Science Basic Research Program of Shaanxi, China (No. 2020JQ-666) and the National Natural Science Foundation of China (Nos. 52004198, 51934009).

References

[1] CAO Pan, ZHANG Shang-hua, ZHENG Ya-jie, HE Han-bing, LAI Shen-zhi, WANG Xing-jun, TAN Bing. Differences of cyanide leaching between calcine and dust from refractory gold concentrates [J]. Transactions of Nonferrous Metals Society of China, 2020, 30: 1964−1979.

[2] WANG Hong-jun, FENG Ya-li, LI Hao-ran, KANG Jin-xing. Simultaneous extraction of gold and zinc from refractory carbonaceous gold ore by chlorination roasting process [J]. Transactions of Nonferrous Metals Society of China, 2020, 30: 1111−1123.

[3] VOLKOV A V, SIDOROV A A. Invisible gold [J]. Herald of the Russian Academy of Sciences, 2017, 87: 40−48.

[4] ARRASCUE M E L, van NIEKERK J. Biooxidation of arsenopyrite concentrate using BIOX® process: Industrial experience in Tamboraque, Peru [J]. Hydrometallurgy, 2006, 83: 90−96.

[5] DENG Tian-long, LIAO Meng-xia. Gold recovery enhancement from a refractory flotation concentrate by sequential bioleaching and thiourea leach [J]. Hydrometallurgy, 2002, 63: 249−255.

[6] MARCHEVSKY N, BARROSO QUIROGA M M, GIAVENO A, DONATI E. Microbial oxidation of refractory gold sulfide concentrate by a native consortium [J]. Transactions of Nonferrous Metals Society of China, 2017, 27(5): 1143−1149.

[7] ZHU Ting-ting, LU Xian-cai, LIU Huan, LI Juan, ZHU Xiang-yu, LU Jian-jun, WANG Ru-cheng. Quantitative X-ray photoelectron spectroscopy-based depth profiling of bioleached arsenopyrite surface by *Acidithiobacillus ferrooxidans* [J]. Geochimica et Cosmochimica Acta, 2014, 127: 120−139.

[8] MÁRQUEZ M A, OSPINA J D, MORALES A L. New insights about the bacterial oxidation of arsenopyrite: A mineralogical scope [J]. Minerals Engineering, 2012, 39: 248−254.

[9] DENG Sha, GU Guo-hua, WU Zi-teng, XU Xiong-yi. Bioleaching of arsenopyrite by mixed cultures of iron-oxidizing and sulfur-oxidizing microorganisms [J]. Chemosphere, 2017, 185: 403−411.

[10] NGOMA E, BORJA D, SMART M, SHAIK K, KIM H, PETERSEN J, HARRISON S T L. Bioleaching of arsenopyrite from Janggun mine tailings (South Korea) using an adapted mixed mesophilic culture [J]. Hydrometallurgy, 2018, 181: 21−28.

[11] ASTUDILLO C, ACEVEDO F. Adaptation of *Sulfolobus metallicus* to high pulp densities in the biooxidation of a flotation gold concentrate [J]. Hydrometallurgy, 2008, 92: 11−15.

[12] ZHANG Duo-rui, XIA Jin-lan, NIE Zhen-yuan, CHEN Hong-rui, LIU Hong-chang, DENG Yu, ZHAO Yi-dong, ZHANG Li-li, WEN Wen, YANG Hong-ying. Mechanism by which ferric iron promotes the bioleaching of arsenopyrite by the moderate thermophile *Sulfobacillus thermosulfido-oxidans* [J]. Process Biochemistry, 2019, 81: 11−21.

[13] FOMCHENKO N V, MURAVYOV M I. Thermodynamic and XRD analysis of arsenopyrite biooxidation and enhancement of oxidation efficiency of gold-bearing concentrates [J]. International Journal of Mineral Processing, 2014, 133: 112−118.

[14] ZHANG Yan, LI Qian, LIU Xiao-liang, YIN Hua-qun, YANG Yong-bin, XU Bin, JIANG Tao, HE Ying-he. The catalytic effect of copper ion in the bioleaching of

arsenopyrite by *Acidithiobacillus ferrooxidans* in 9K culture medium [J]. Journal of Cleaner Production, 2020, 256: 120391.
[15] JIN Jian, SHI Shao-yuan, LIU Guo-liang, ZHANG Qing-hua, CONG Wei. Arsenopyrite bioleaching by *Acidithiobacillus ferrooxidans* in a rotating-drum reactor [J]. Minerals Engineering, 2012, 39: 19−22.
[16] ZHANG Xu, FENG Ya-li, LI Hao-ran. Enhancement of bio-oxidation of refractory arsenopyritic gold ore by adding pyrolusite in bioleaching system [J]. Transactions of Nonferrous Metals Society of China, 2016, 26: 2479−2484.
[17] DENG Sha, HE Guo-shuai, WU Bi-chao, GU Guo-hua. Pyrite-promoted dissolution of arsenopyrite in the presence of *Sulfobacillus thermosulfidooxidans* [J]. Journal of Materials Research and Technology, 2020, 9: 9362−9371.
[18] FANG Fang, ZHONG Hong, JIANG Fang-ming, LUO Zhong-yin, SUN Xiao-wei, XU Kai-yang. Effect of pyrite on bioleaching of arsenopyrite [J]. The Chinese Journal of Nonferrous Metals, 2013, 23(10): 2970−2976. (in Chinese)
[19] TAXIARCHOU M, ADAM K, KONTOPOULOS A. Bacterial oxidation conditions for gold extraction from Olympias refractory arsenical pyrite concentrate [J]. Hydrometallurgy, 1994, 36: 169−185.
[20] KOMNITSAS K, XENIDIS A, ADAM K. Oxidation of pyrite and arsenopyrite in sulphidic spoils in Lavrion [J]. Minerals Engineering, 1995, 8: 1443−1454.
[21] URBANO G, REYES V E, VELOZ M A, GONZáLEZ I. Pyrite−arsenopyrite galvanic interaction and electrochemical reactivity [J]. The Journal of Physical Chemistry C, 2008, 112: 10453−10461.
[22] DOS SANTOS E C, LOURENÇO M P, PETTERSSON L G M, DUARTE H A. Stability, structure, and electronic properties of the pyrite/arsenopyrite solid–solid interface—A DFT study [J]. The Journal of Physical Chemistry C, 2017, 121: 8042−8051.
[23] XU Jia-ning, SHI Wen-ge, MA Peng-cheng, LU Liang-shan, CHEN Gui-min, YANG Hong-ying. Corrosion behavior of a pyrite and arsenopyrite galvanic pair in the presence of sulfuric acid, ferric ions and HQ0211 bacterial strain [J]. Minerals, 2019, 9: 169.
[24] DENG Sha, GU Guo-hua, HE Guo-shuai, LI Li-juan. Catalytic effect of pyrite on the leaching of arsenopyrite in sulfuric acid and acid culture medium [J]. Electrochimica Acta, 2018, 263: 8−16.
[25] BLANEY L. Magnetite (Fe_3O_4): Properties, synthesis, and applications [J]. Lehigh Review, 2007, 15: 33−81.
[26] SAAVEDRA A, GARCÍA-MEZA J V, CORTÓN E, GONZÁLEZ I. Understanding galvanic interactions between chalcopyrite and magnetite in acid medium to improve copper (bio)leaching [J]. Electrochimica Acta, 2018, 265: 569−576.
[27] HUAI Yang-yang, PLACKOWSKI C, PENG Yong-jun. The surface properties of pyrite coupled with gold in the presence of oxygen [J]. Minerals Engineering, 2017, 111: 131−139.
[28] DENG Sha, GU Guo-hua. An electrochemical impedance spectroscopy study of arsenopyrite oxidation in the presence of *Sulfobacillus thermosulfidooxidans* [J]. Electrochimica Acta, 2018, 287: 106−114.
[29] NESBITT H W, MUIR I J, PRARR A R. Oxidation of arsenopyrite by air and air-saturated, distilled water, and implications for mechanism of oxidation [J]. Geochimica et Cosmochimica Acta, 1995, 59: 1773−1786.
[30] CORKHILL C L, WINCOTT P L, LLOYD J R, VAUGHAN D J. The oxidative dissolution of arsenopyrite (FeAsS) and enargite (Cu3AsS4) by *Leptospirillum ferrooxidans* [J]. Geochimica et Cosmochimica Acta, 2008, 72: 5616−5633.

酸性培养基体系中磁铁矿对砷黄铁矿电化学氧化的原电池效应

邓 莎[1]，顾帼华[2]，龙 涛[1]，肖 巍[1]，杨 玮[1]

1. 西安建筑科技大学 资源工程学院，西安 710055；
2. 中南大学 资源加工与生物工程学院，长沙 410083

摘 要：采用电化学测试、XPS 和浸出试验，研究酸性培养基体系中砷黄铁矿与磁铁矿之间的原电池效应。结果表明，磁铁矿的静电位为 321 mV，高于砷黄铁矿的 223 mV，两者之间的原电池电流为 7.40 μA，证明砷黄铁矿和磁铁矿之间确实存在原电池效应。原电池电位和极化曲线表明，砷黄铁矿的氧化还原行为在整个原电池反应中占主导地位，原电池反应可强化砷黄铁矿的电化学溶解，促进表面氧化产物（S^0, SO_3^{2-}, SO_4^{2-}和 AsO_3^{3-}）的生成，提高砷黄铁矿表面的化学反应活性。6 d 的浸出试验表明，在磁铁矿存在下，砷黄铁矿中砷的溶出浓度提高 30 mg/L，进一步证明磁铁矿对砷黄铁矿的氧化具有强化作用。

关键词：砷黄铁矿；磁铁矿；原电池效应；电化学；表面性质；浸出

(Edited by Bing YANG)